Bering Strait Transports from Satellite Altimetry

J. Y. Cherniawsky, W. R. Crawford, O. Nikitin* and E. C. Carmack

Institute of Ocean Sciences, Fisheries and Oceans Canada, Sidney, BC
*State Oceanographic Institute, Moscow, Russia

Abstract

TOPEX/POSEIDON altimetry data are used to compute sea level slopes across the Bering Strait and associated geostrophic transport anomalies through the strait during ice-free periods from 1992 to 2002. The satellite turning latitude near 66°N is just north of the strait, allowing us to use data from seven nearly zonal altimeter tracks close to the strait and to provide estimates of mean slopes, geostrophic currents and water transports approximately every 1.5 days. The altimeter-derived transport anomalies far exceed the mean value and are in good agreement with those derived from in-situ observations. Comparison to wind data from a nearby meteorological station in Uelen, Russia, shows the computed transport anomalies to correlate well with strong along-strait winds and less so with winds from other directions, thus making the transport predictions from winds alone more successful in seasons with strong and persistent meridional winds.

Corresponding author: Josef Cherniawsky, Institute of Ocean Sciences, P.O. Box 6000, Sidney, B.C., Canada V8L 4B2, email: CherniawskyJ@pac.dfo-mpo.gc.ca

1 Introduction

Water transport through Bering Strait modifies water mass characteristics in the Arctic Ocean and is one of key factors affecting the fresh-water budget in the Arctic and stability of the Atlantic overturning circulation (Coachman et al. 1975; Aagaard and Carmack 1989; Goose et al. 1997; Shimada et al. 2001; De Boer and Nof 2004; Woodgate and Aagaard 2005b). Direct observations of this transport are limited to measurements of velocity at a few stations in the strait, or occasional sections of temperature and salinity across it (Coachman and Aagaard 1966; Coachman and Aagaard 1981; Roach et al. 1995; Woodgate and Aagaard 2005a), which provide basic knowledge about the mean transport and its variability.

One of the first (if not the first) oceanographic investigations of this transport was by Ratmanov (1937), who used current meter data from the summers of 1932 and 1933 to show that the prevailing flow is to the north, with an average velocity of about 50 cm s^{-1}, ranging in the vertical between 35 and 60 cm s^{-1}. Such early results from the Russian cruises in the 1930s and 1940s were reviewed by Shtokman (1957), who also analyzed the likely causes of the northward flow through the strait. He concluded that this flow is composed of two parts: the wind-driven part, due to an average wind stress, and another part that is independent of the wind and is due to a meridional pressure gradient in the strait, caused by differences in water density between the Bering and Chukchi Seas. The latter mechanism was previously suggested by Jacobs (1951), who attributed the meridional density gradient to differences in evaporation minus precipitation between the two basins. Shtokman's conclusions agree with modern theory that the long-term Bering Strait transport is maintained by sea level difference between Pacific and Arctic Oceans, as well as location of semi-permanent atmospheric pressure systems (Coachman and Aagaard 1966; Coachman et al. 1975; Roach et al. 1995).

Early estimates of transport through Bering Strait were made by a number of Russian investigators, with monthly and annual values presented in Table 1 in Fedorova and Yankina (1963). The latter also used monthly mean measurements

over the period of 1941-1961, computing an annual mean speed of 40 cm s^{-1} and volume transport of 0.95 Sv (1 Sverdrup = 10^6 m^3s^{-1}). More recently this transport was estimated to be about 0.8 Sv, with a mean annual amplitude of 0.5 Sv, peaking in July (and a secondary peak in January), and interannual variation of $\pm$0.3 Sv (Roach et al. 1995). The transport is larger, about 1.0 Sv, in the summer (June–November). The shorter duration (days to months) fluctuations are mostly due to changes in synoptic winds near the strait. The winds have a systematic effect on the flow, as without them, the mean transport is expected to be near 1.1 Sv (Roach et al. 1995). Indeed, up to two-thirds of the transport variance can be explained by the surface geostrophic wind (Aagaard et al. 1985; Roach et al. 1995) and during periods of persistent northerly winds, this flow can be reversed (Coachman and Aagaard 1988; Melling 2000).

While direct measurements are difficult, satellite data can give valuable information on the flow. Figure 1 shows an example of surface water color, which is an indicator of chlorophyll abundance, tracing the northward flow in the strait. Such optical images are only possible during cloud-free periods. However, radar altimeters from orbiting satellites provide all-weather observations of sea level in the strait. According to Roach et al. (1995), the autocorrelation of the observed transport timeseries has a mean e-folding time scale of about 4.5 days, which has important implications for using satellite altimetry data. In the following sections we describe wind data and the measurements of sea level gradients by altimeters aboard the TOPEX/POSEIDON (TP) satellite, their utility in calculation of water transports through the Bering Strait, and the nature of the relation between these transports and the winds in the strait.

2 Wind data

The wind time series used in this study are from the Uelen Hydrometeorological Station (66°5′N, 169°39′W). It is located on the north shore of the Chukotsky Peninsula, on a 300-m wide pebble spit, about 100 m from the north coast and only 12 km from Cape Dezhneva (66°10′N, 169°50′W). The base of the 12-m high anemometer tower

is at 6.6 m above sea level. Because of the low relief around this station (except for a single rise near Cape Dezhneva, about 10 km away) and its relative proximity to the Bering Strait, these data are assumed to be representative of the winds in the strait. The 6-hourly observations of wind speed and direction were interpolated in time to coincide with the available TP data during ice-free periods, October 1992 until July 2002. Figure 2 shows the directional distribution of winds at Uelen for ice-free periods (June to November) during 1992–2002, with colored wedges showing relative occurrence (in %) in three different wind strength categories: weak, moderate and strong. The striking feature is the north-south orientation of the winds, with somewhat more prevalent and stronger winds from the north.

3 Altimeter data

The TOPEX/POSEIDON (TP) altimeter data were obtained from Brian Beckley and Richard Ray of the NASA Pathfinder Project [private communication]. Standard instrumental and geophysical corrections, except for the ocean tides, were made at the Goddard Space Flight Center (Koblinsky et al. 1999) and the resulting, so-called *tidalist* version of altimeter data were processed at the Institute of Ocean Sciences. Tidal constants were computed using enhanced least-squares harmonic analysis method (Cherniawsky et al. 2001), modified from a standard tidal analysis package (Foreman 1977). The overdetermined least-squares problem was solved using singular-value decomposition, which also provides estimates of expected errors in these constants. Bering Strait is under seasonal ice cover, leaving 5-6 months, June to November, with usable data for the analysis (Fig. 3). We used a reduced set of 10 tidal coefficients (Z_0, Q_1, O_1, P_1, K_1, $_2N_2$, N_2, M_2, S_2 and K_2), compared to 21 in Northeast Pacific (Cherniawsky et al. 2001). Diurnal and semi-diurnal gravitational tides are generally small in Bering Strait, much smaller than storm surges, or longer-period variability.

The residual (non-tidal) signals are very large over the shallow Bering Sea shelf, mainly due to sea level response (surges) to passing storms. An example of detided sea level anomalies during a single 10-day TP cycle (Fig. 4) shows large (positive

and negative) storm-driven sea level signals in the northern Bering Sea. The 10-day cycle is too long to resolve individual storms, which explains why some neighboring tracks (in space, not in time) exhibit large anomalies of opposite sign.

The TP satellite turning latitude near 66°10'N is just north of Bering Strait, giving seven tracks in that area oriented almost directly across the strait (framed area in Fig. 3b) and providing east-west sea level gradients seven times in each 10-day TP cycle during ice-free periods. This fortunate location of the turning latitude and the 4.5-day autocorrelation time scale for the measured transports (Roach et al. 1995) permit us to resolve the individual storm events and to compute both synoptic and lower-frequency variability of the Bering Strait throughflow. Large sea level signals on the shelf and the use of sea-level gradients help to compensate for possible errors in large-scale atmospheric corrections and satellite orbits at these high latitudes.

4 Calculation of transports

For this short strait, we can ignore the frictional effects (e.g., Melling (2000)). Using standard notation, we can partition the northward surface velocity in the strait, $v(x,z)$ at $z=0$, into barotropic and baroclinic parts

$$v(x,0) = v_{bt}(x) + v_{bc}(x,0) = \frac{g}{f}\frac{\partial \eta}{\partial x} \tag{1}$$

where the barotropic part v_{bt} is the depth-averaged velocity, while the baroclinic part denotes the surface geostrophic current

$$v_{bc}(x,0) = \frac{1}{f}\frac{\partial D'(x,0)}{\partial x} \tag{2}$$

due to dynamic height anomaly $D'(x,0) = D(x,0) - \bar{D}(x)$, where $\bar{D}(x)$ is the depth-mean value of $D(x,z)$ (Fofonoff 1963; Lyu and Kim 2003). For a given channel profile of width L and average depth H, we get the northward water transport

$$T_y = H\int_0^L v_{bt}(x)dx = H\int_0^L \left[\frac{g}{f}\frac{\partial \eta}{\partial x} - v_{bc}(x,0)\right] dx \tag{3}$$

We now assume that over the full width of the channel, the barotropic transport dominates the flow, $\left|\int_0^L v_{bc}(x,0)dx\right| \ll \left|\int_0^L v_{bt}(x)dx\right|$, which may be justifiable for a number of reasons. Because of the small internal Rossby radius at these latitudes, the baroclinic currents are usually confined to narrow bands ($\sim$ 10 km wide) near each coast and are missed by altimetry data. Also, such currents contribute no more than 20% to the total transport (e.g., Roach et al. (1995); Woodgate and Aagaard (2005a)). Notably, such approximation also holds at low latitudes, where vertical stratification is stronger than in the Bering Strait (see for example Fig. 4 in Lyu and Kim (2003)). Additional evidence for an essentially barotropic flow in the channel comes from ship ADCP data, showing the 40-m deep velocity to be a fair representation of the depth-mean velocity and that the assumption of a vertically uniform flow is reasonably good, within 10-20% (Roach et al. 1995; Woodgate et al. 2005). This gives an approximate transport

$$T_y \approx H \int_0^L \frac{g}{f}\frac{\partial \eta}{\partial x}dx = \frac{gH}{f}\left[\eta(L) - \eta(0)\right] \approx \frac{gHL}{f}\frac{\Delta\eta}{\Delta x} \tag{4}$$

as a function of sea level slope across the strait. Due to somewhat different locations of the seven TP tracks (Fig. 3) and likely missing data, we do not have sea level values at $x = 0$ and $x = L$ (see also Fig. 6 below). We therefore use a linear fit for the slope $\Delta\eta/\Delta x$ from available data in each TP track.

Figure 5 shows "local" sea level anomalies in Bering Strait for each ice-free TP cycle, from the last week of September, 1992, until the first week of August, 2002. Alongtrack mean values were subtracted, thus showing only the slopes. The calculated northward transport anomalies are displayed in the right panel for an average depth of $H = 50$ m and channel width $L = 90$ km (realistic values at 66°N, see Fig. 3b), with an assumed summer-mean transport value of 1 Sv marked as a –1 Sv bias (dashed line) in Fig. 5. The transport is therefore taken to be positive (to the north) if its anomaly exceeds –1 Sv.

There are several interesting features in Fig. 5. It shows visible, though varying, temporal correlation of the order of days to weeks in the slopes and associated transports, most likely due to persistent pressure and wind systems. The transports are

usually higher in the beginning and middle of each ice-free season, then decreasing and becoming more variable towards the end of the season. Indeed, in all years, except for 1995, there are significant transport reversals ($T_y < -1$ Sv) each fall due to seasonal shifts to stronger northerly winds. Fig. 6 displays an expanded view for 1996, also showing the wind components U and V. It is quite apparent that in this year, a significant correspondence exists between V and the transport. This relationship is the subject of the next section.

5 Complex relation between transports and winds

It is well known that short-term variations in Bering Strait transport are well correlated with local winds. We can write the TP-derived transport estimates $\mathbf{T}$ as a linear system

$$\mathbf{T} = C\mathbf{W} + \mathbf{R} \tag{5}$$

where $\mathbf{T} = \mathbf{T}_x + i\mathbf{T}_y$, $C = C_x + iC_y$ is a complex coefficient, $\mathbf{W} = \mathbf{W}_x + i\mathbf{W}_y$ is the wind time series (in complex notation), $\mathbf{R}$ is a complex residual vector, and we assign small random values to across strait $\mathbf{T}_x$. Given a sufficient number of T_{yi} ($i = 1, \ldots, N$) and coincident wind observations (W_{xi}, W_{yi}), we calculate a least-squares solution for the unknown transfer function C by minimizing the residual

$$\chi^2 = |C\mathbf{W} - \mathbf{T}|^2 \tag{6}$$

while using the singular value decomposition (SVD) method. For all ice-free observations during October 1992 – August 2002 ($N = 753$), we get

$$C = 0.071 - i0.004 \tag{7}$$

in units of Sv$(\mathrm{ms}^{-1})^{-1}$, giving a small rotation angle $\alpha = -3.5°$, i.e. "to the right" of the wind. The 2×2 correlation coefficients between wind and water transport components

$$(S_{xx}, S_{xy}, S_{yx}, S_{yy}) = (-0.038, -0.000, -0.004, 0.608) \tag{8}$$

show a relatively strong correlation in the north-south direction. Given the large number of data pairs (N), this value of S_{yy} is significant on the 1% level (based on the standard error $\sigma_z = 1/\sqrt{N'-4} = 0.064$ of the normalized population variable $z = \frac{1}{2}[\ln(1+S_{yy}) - \ln(1-Syy)] = 0.706$, where $N' = N/3$ due to the autocorrelation time scale of 4.5 days). Indeed, the prevailing winds in the strait are along this direction (Fig. 2) and the meaning of α is the resultant angle of these winds relative to the north, as we assumed our T_{yi} to be along this direction.

The average transfer coefficient C calculated above actually depends on wind range considered in its calculation. In the above calculation, we used all winds larger than a small minimum value of 2 m s^{-1}. If this threshold is increased, C and S_{yy} increase as well (though N, naturally, decreases), which just says that stronger winds have larger influence on the transports. The skill of the hindcast is commonly defined as $\gamma = 1 - \langle (C\mathbf{W} - \mathbf{T})^2 \rangle \,/\, \langle \mathbf{T}^2 \rangle$, where $\langle \cdot \rangle$ denotes time averaging operator. The computed γ has an average value of 0.335 and also increases with wind speed.

The dependence of the transfer coefficient and of other fitted parameters on the strength of the wind is also visible in Fig 7, which shows the results of the above least-squares fit, but done separately for each ice-free season. Excluding the years 1992 and 2002, which did not have enough samples ($N < 30$), we notice that in the years when the average meridional wind speed is relatively low, the transfer coefficient C, the meridional correlation S_{yy}, and the skill γ are also low. During this time period, the year 1995 has the "worst" predictability from winds alone, while 1996 and 2001 appear to be the "best" from this point of view. Indeed, the "predicted" transport $C\mathbf{W}$ in 1996 follows quite closely the "measured" transport $\mathbf{T}_y$, shown in Fig 6.

6 Discussion

The Bering Strait transport anomaly results from TP altimetry data appear to be in general agreement with those based on in-situ data. However, several approximations were used in these calculations, some of which were mentioned above. These

include (a) collocation of the altimetry tracks onto a single latitude circle (66°N; see Fig 3b), (b) "missing" up to 20 % of transport that may be contained in the baroclinic part of the flow (section 4), including the contributions from narrow coastal jets not resolved by altimetry data, (c) assumption of a single rectangular crossection for the strait, with fixed width (90 km) and depth (50 m), and (d) a linear slope representation for the sea surface across the strait.

Other likely sources of error arise from processing TP data in an area with partial ice cover. Fortunately, some of the typical errors that affect altimetry-derived sea levels, such as errors in satellite orbit, or in atmospheric data (sea level pressure, sea-state, etc.) have a large-scale signature and are therefore expected to have a minor effect on fitted slope anomalies across the relatively narrow strait. Therefore, in spite of the reduced number of tidal constituents used to detide TP data, the residual sea level anomaly errors are considered here to be less than 4 cm and relative errors in individual slope anomalies to be of the same order, about 4 cm over a 90 km width, which is about 10-20% of the typical slope values (see Fig. 6).

The above assumptions and characteristics of the data sets used here affect the computed value of the average transfer coefficient (scaling) $|C|$, which was found to be 0.071 $\mathrm{Sv}(\mathrm{ms}^{-1})^{-1}$ for all of the 1992-2002 ice-free periods. This is smaller than the 0.11-0.12 values (Coachman and Aagaard 1988; Roach et al. 1995), based mostly on winter data. Knowing that this scaling increases in years with stronger winds (Fig. 7), it is not surprising that the winter-based value is larger, as the winds are stronger in winter, while our average scaling was adversely affected by several "poor" years, such as 1995, 1998 and 2002. The assumed geometry of the strait at 66°N is also different from the actual Bering Strait cross-section used in Roach et al. (1995). Because of the unknown "missing" baroclinic contribution, the TP-derived transport anomalies may be somewhat too small, which would also lower the scaling $|C|$. In addition, the above authors used geostrophic winds, calculated from atmospheric pressure maps, while Uelen station winds are from a coastal tower, about 18 m above sea level, implying an unknown scaling between the two data sets.

Notably, the direct effect of wind forcing, investigated here and in previous works

on Bering Strait, is also related to forcing the flow by the along-strait pressure (sea level) gradient, as the latter can be set-up by the prevailing winds (e.g., Garrett and Toulany (1980); Hannah and Crawford (1996)), in addition to that due to the meridional water density gradient. It is not always possible to distinguish between pressure and wind-driven mechanisms, especially if both processes produce a similar response in a strait. For example, Crawford et al. (1988) found the transport in Hecate Strait (British Columbia) to lag about 6 hours behind large-scale winds. Given the dimensions and the average depth of that strait, this lag is consistent with either direct forcing by wind, or from along-strait pressure gradient, or both. However, it may take longer to set up a large-scale sea level gradient over the very wide and shallow Bering and Chukchi Seas shelves than to force the flow in Bering Strait directly with the wind.

The local adjustment time scale to direct wind forcing is about one half of the inertial period, or just over 6 hours at this latitude, while the speed of large-scale wind set up is defined by the time it takes to create a sea level surge at the coast, when onshore Ekman transport is balanced by bottom friction. Assuming a mainly barotropic flow on the shallow shelf, the frictional spin-up, or spin-down time scale is given by $t_{spin} = (1 + f^2/\kappa^2 c^2)H/2C_D u_{av}$ (see par. 9.12 in Gill (1982)), where $c = \sqrt{gH} \approx 20$ m s^{-1} for a 40-m deep shelf, κ is the horizontal wave number, i.e. an inverse of a length-scale for a pressure cell on the shelf, assumed to be about $\kappa^{-1} \sim 200$ km ($\kappa = 2\pi/L$, where $L > 1000$ km, i.e., more than twice the width of the shelf), and we use the values $C_D = 0.0025$ and $u_{av} = 0.4$ m s^{-1}. For this value of κ^{-1} and the barotropic Rossby radius $c/f \approx 150$ km, we get $t_{spin} \approx 16$ hours, quite longer than the inertial spin-up (~ 6 hours) or the purely frictional time scale $H/2C_D u_{av} \approx 5.6$ hours.

To resolve this issue, we did a lag-correlation analysis between the wind and transport time series – by shifting the wind data by up to ± 24 hours, at 3-hour intervals. This produced relative broad maxima (not surprising, given the 1.5-day sampling interval) in S_{yy} and γ for lag value between +3 and +6 hours (the transport lags the wind), with both of these only slightly higher (0.609 and 0.339) than their

values at zero lag. For time lag values beyond +12, or −3 hours, there was a more rapid decrease in both of these parameters, as well as a gradual decrease in the scaling $|C|$. If the above assumptions are correct, then this time lag analysis indicates that the observed synoptic variability of the transport in the strait is more affected by the local wind than by large scale pressure gradients.

7 Conclusions

We successfully used the TOPEX/POSEIDON altimetry data to compute sea level slopes across the Bering Strait and associated transport anomalies through the strait during ice-free periods from 1992 to 2002. The satellite turning latitude near 66°N allowed us to provide estimates of mean slopes, geostrophic currents and water transports at approximately 1.5-day intervals. The altimeter derived transport anomalies are in relatively good agreement with those derived from in-situ observations. Comparison to wind data from a nearby meteorological station in Uelen, Russia, shows the computed transport anomalies to correlate well with strong winds oriented along the axis of the strait. Therefore the transport predictions from winds alone are more successful during the years with strong meridional winds, when the meridional correlation coefficient exceeds 0.6 and the predictive skill is larger than 0.4. A rudimentary time-lag analysis indicates that the Bering Strait transport lags the Uelen winds by about 3 to 6 hours, which seems to favor the more direct wind forcing mechanism for this synoptic variability, compared to a forcing by a large scale sea level gradient.

Acknowledgements We are grateful to Richard Ray (GSFC/NASA) and Brian Beckley (Raytheon Corp.) for providing the *tidalist* version of the Pathfinder altimetry data and to the Russian Hydrometeorological Service for making available the Uelen wind data. Communications with Rebecca Woodgate and Knut Aagaard of the Pacific Marine Environment Laboratory (NOAA) and with Patrick Cummins, Humfrey Melling and Mike Foreman of the Institute of Ocean Sciences (DFO) were very helpful. This work was supported in part by the Canadian Panel on Energy, Research and Development, PERD CCIS project DFO-0602.

References

Aagaard, K. and E. C. Carmack (1989). The role of sea ice and other fresh water in the Arctic circulation. *J. Geophys. Res. 94*, 14,485–14,498.

Aagaard, K., A. T. Roach, and J. D. Schumacher (1985). On the wind-driven variability of the flow through Bering Strait. *J. Geophys. Res. 90*, 7213–7221.

Cherniawsky, J. Y., M. G. G. Foreman, W. R. Crawford, and R. F. Henry (2001). Ocean tides from TOPEX/Poseidon sea level data. *J. Atmos. Oceanic Technol. 18*, 649–664.

Coachman, L. K. and K. Aagaard (1966). On the water exchange through Bering Strait. *Limnol. Oceanogr. 11*, 44–59.

Coachman, L. K. and K. Aagaard (1981). Re-evaluation of water transports in the vicinity of Bering Strait. In D. W. Hood and J. A. Calder (Eds.), *The Eastern Bering Sea Shelf: Oceanography and Resources, Vol. I*, pp. 95–110. Washington, DC: NOAA.

Coachman, L. K. and K. Aagaard (1988). Transports through Bering Strait: Annual and interannual variability. *J. Geophys. Res. 93*, 15,535–15,539.

Coachman, L. K., K. Aagaard, and R. B. Tripp (1975). *Bering Strait: The Regional Physical Oceanography*. University of Washington Press, Seattle, WA. 172 pp.

Crawford, W. R., W. S. Huggett, and M. J. Woodward (1988). Water transport through Hecate Strait, British Columbia. *Atmos.-Ocean 26*, 301–320.

De Boer, A. M. and D. Nof (2004). The Bering Strait's grip on the northern hemisphere climate. *Deep-Sea Res., Part I, 51*, 1347–1366.

Fedorova, Z. P. and Z. S. Yankina (1963). Supply of Pacific Ocean water through Bering Strait into Chukchi Sea. *Okeanologiya 3*, 777–784. (In Russian).

Fofonoff, N. P. (1963). Dynamics of ocean currents. In M. N. Hill (Ed.), *The Sea, Vol. 1*, pp. 323–395. New York: John Wiley.

Foreman, M. G. G. (1977). Manual for Tidal Heights Analysis and Prediction. *Pacific Marine Science Report 77-10*. Institute of Ocean Sciences, Sidney, B.C., Canada, 101 pp.

Garrett, C. and B. Toulany (1980). Variability of the flow through the Strait of Belle Isle. *J. Mar. Res. 39*, 163–189.

Gill, A. E. (1982). *Atmosphere-Ocean Dynamics*. New York: Academic Press. 662 pp.

Goose, H., J. M. Campin, T. Fichefet, and E. Deleersnijder (1997). Sensitivity of a global ice-ocean model to the Bering Strait throughflow. *Climate Dyn. 13*, 349–358.

Hannah, C. G. and W. R. Crawford (1996). Winter transport and sea level fluctuations in Hecate Strait, British Columbia. *J. Geophys. Res. 101*, 28,365–28,376.

Jacobs, W. C. (1951). The energy exchange between sea and atmosphere and some of its consequences. *Bull. Scripps Inst. Oceanogr. 6*, 27–122.

Koblinsky, C. J., R. Ray, B. D. Beckley, Y. M. Wang, L. Tsaoussi, A. Brenner, and R. Williamson (1999). NASA Ocean Altimeter Pathfinder Project, Report 1: Data Processing Handbook. Technical Report NASA/TM-1998-208605, NASA/GSFC.

Lyu, S. J. and K. Kim (2003). Absolute transport from the sea level across the Korea Strait. *Geophys. Res. Lett. 30*, 1285, doi:10.1029/2002GL016233.

Melling, H. (2000). Exchanges of freshwater through the shallow straits of the North American Arctic. In E. L. Lewis et al. (Ed.), *The Freshwater Budget of the Arctic Ocean, Proc. NATO Adv. Res. Workshop, Tallin, Estonia, 27 April – 1 May 1998*, Dortrecht, pp. 479–502. Kluwer.

Ratmanov, G. E. (1937). On the question of water exchange through Bering Strait. *Issledovaniya Morei SSSR 25*, 119–135. (In Russian).

Roach, A. T., K. Aagaard, C. H. Pease, S. A. Salo, T. Weingertner, V. Pavlov, and M. Kulakov (1995). Direct measurements of transport and water properties through the Bering Strait. *J. Geophys. Res. 100*, 18,443–18,457.

Shimada, K., E. C. Carmack, K. Hatakeyama, and T. Takizawa (2001). Varieties of shallow temperature maximum waters in the western Canadian Basin of the Arctic Ocean. *Geophys. Res. Lett. 28*, 3441–3444.

Shtokman, V. B. (1957). Influence of wind on the current in the Bering Strait, causes of their large velocity and predominantly northward direction. *Trudy Instituta Okeanologii im. P. P. Shirshova, Akademia Nauk SSSR 25*, 171–191. In Russian; translated by L. B. Coachman, Dept. Oceanography, Univ. of Washington, Seattle, WA.

Woodgate, R. A. and K. Aagaard (2005a). Monthly temperature, salinity and transport variability of the Bering Strait throughflow. *Geophys. Res. Lett. 32*, L04601, doi:10.1029/2004GL021880.

Woodgate, R. A. and K. Aagaard (2005b). Revising the Bering Strait freshwater flux into the Arctic Ocean. *Geophys. Res. Lett. 32*, L02602, doi:10.1029/2004GL021747.

Woodgate, R. A., K. Aagaard, and T. Weingartner (2005). A year in the physical oceanography of the Chukchi Sea: Moored measurements from Autumn 1990-1991. *Deep-Sea Res. 52*. in press.

Figure 1: MISR (Terra satellite) image of the Bering Straits on August 18, 2000, showing meandering northward flow originating south of the strait (courtesy NASA/GSFC/JPL).

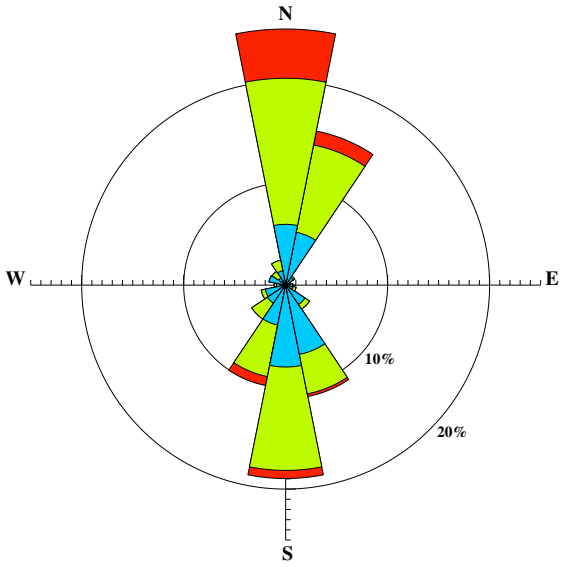

Figure 2: Directional distribution of winds at Uelen, Russia, during June-November, 1992-2002, with each segment showing relative occurrence (in %) of winds *from* that direction. Blue, green and red color wedges partition these segments into 3 wind speed categories, weak: $2.0 - 8.2$ ms^{-1}, medium: $8.2 - 13.4$ ms^{-1}, and strong: > 13.4 ms^{-1} (these speed values correspond to 4, 16 and 27 knots, respectively).

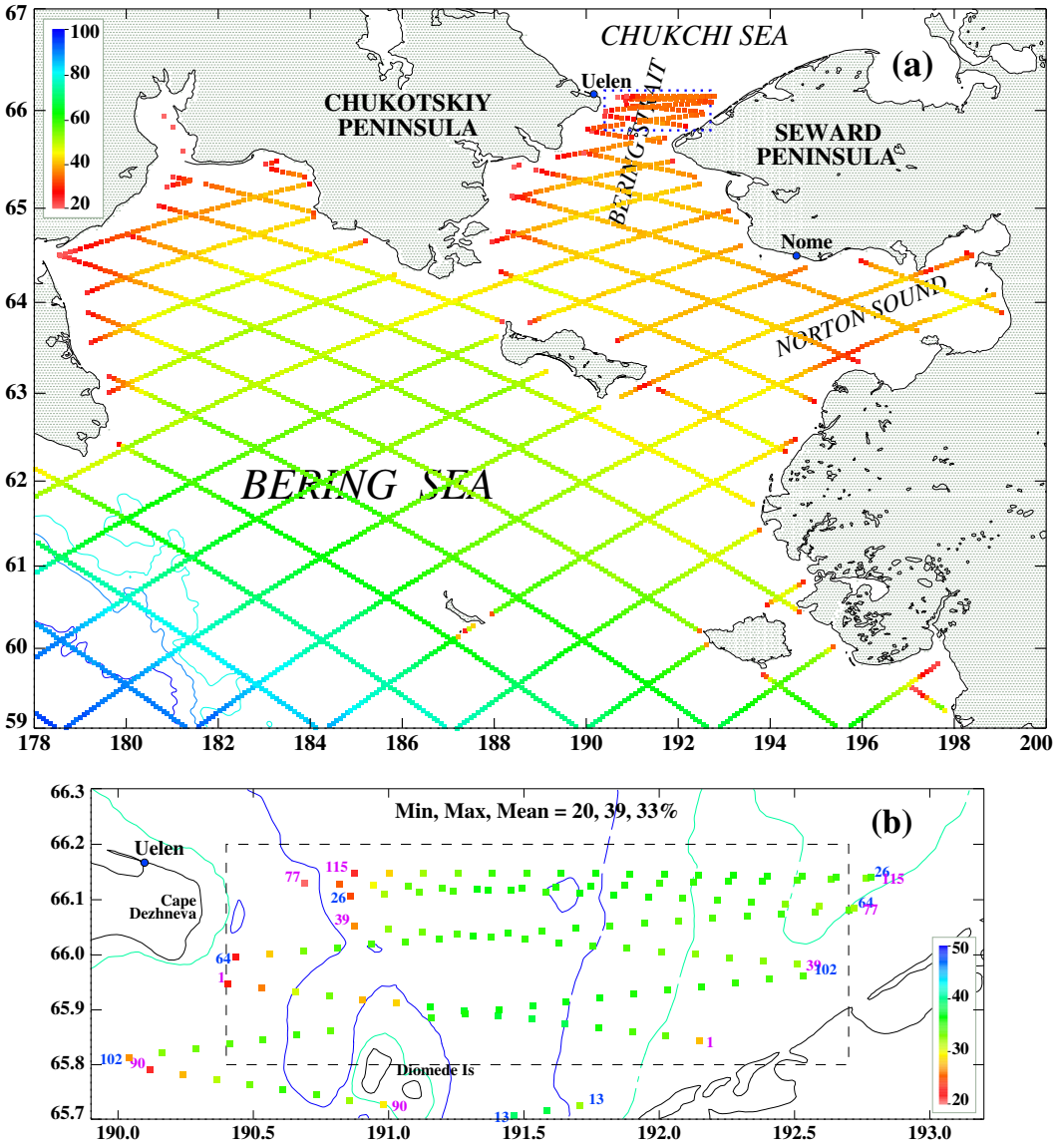

Figure 3: TOPEX/POSEIDON (TP) altimeter data coverage (in %) (a) in north-eastern Bering Sea and (b) in Bering Strait area. Bathymetric contours of 200, 1000 and 3000 m are shown in (a) and 20 and 50 m in (b). The dashed frame in (b) encloses the seven TP tracks in Bering Strait used in this study, with ascending (descending) track numbers printed in blue (purple).

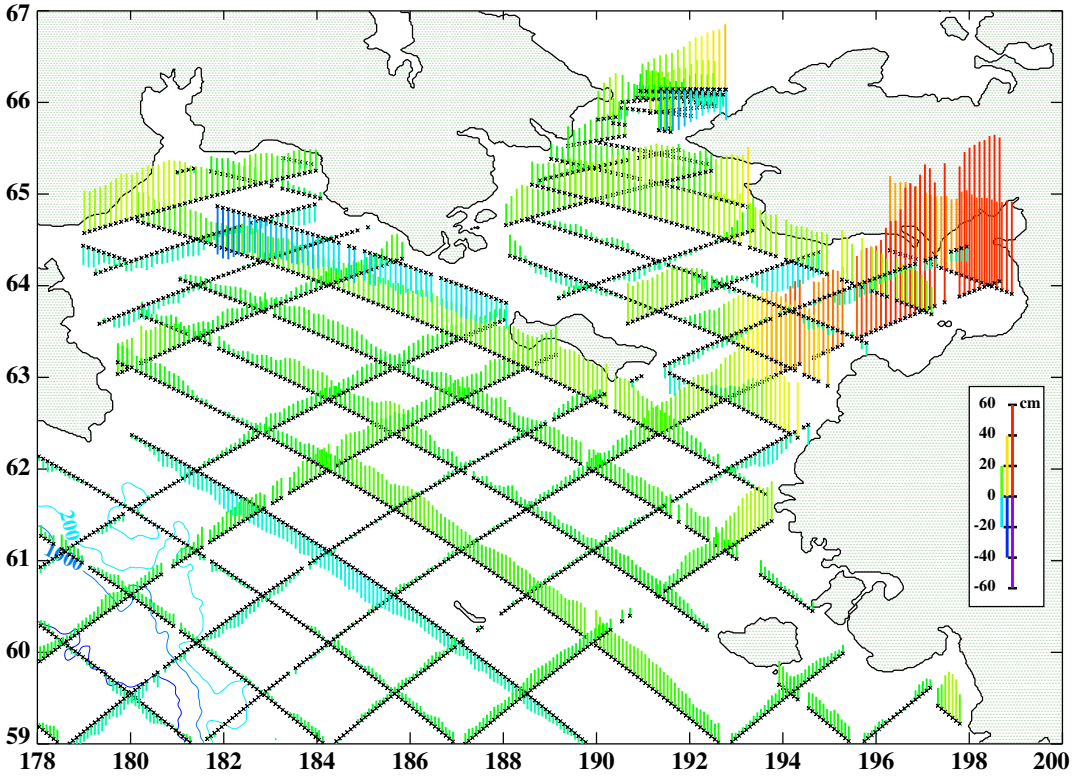

Figure 4: Example of TP sea level anomalies during one 10-day cycle: Sep. 8–17, 2001.

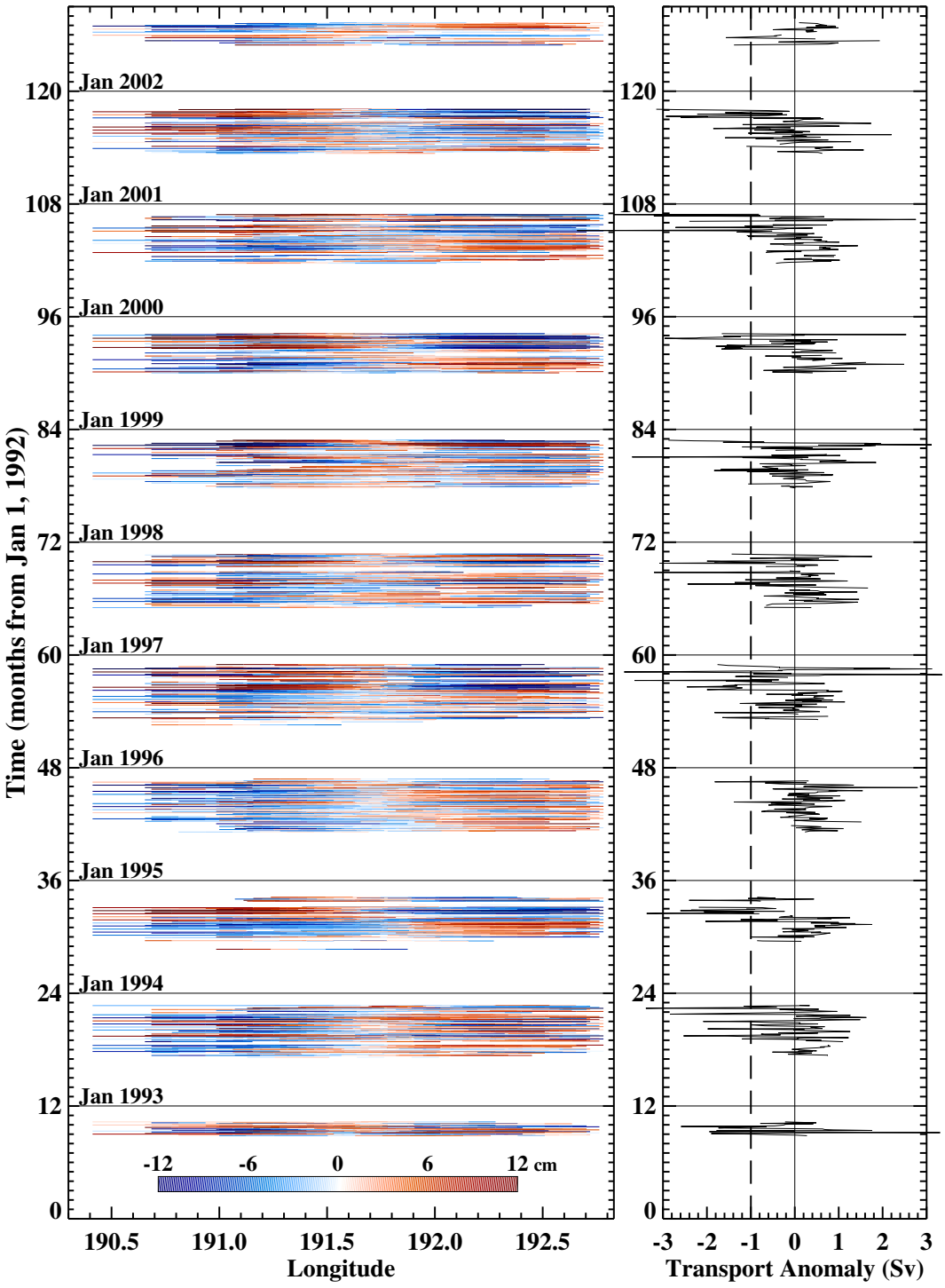

Figure 5: "Local" sea level anomalies (in cm) and computed transport anomalies (in Sv) in the Bering Strait from TP data during ice-free periods, 1992–2002 (dashed line: a bias of 1 Sv).

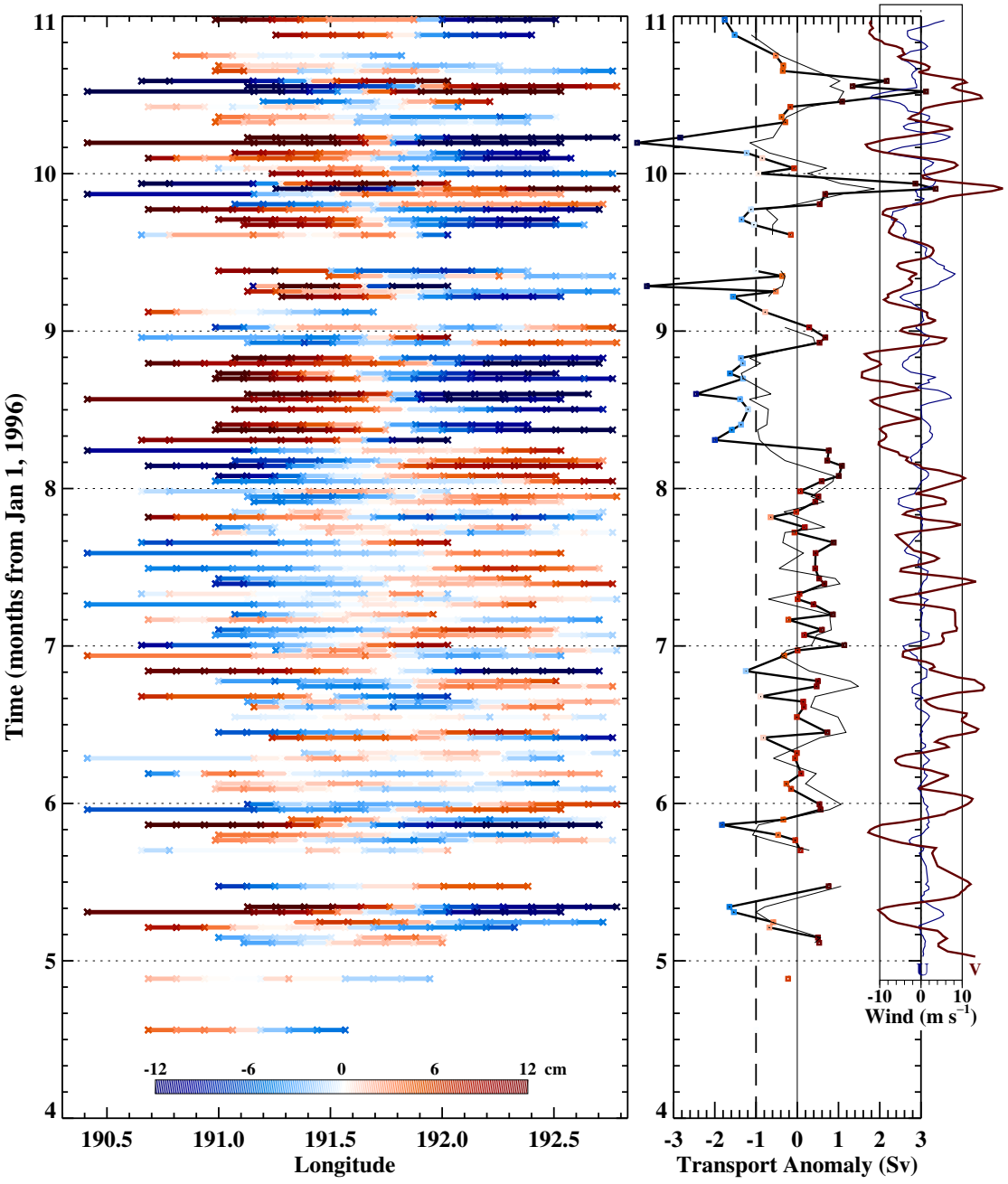

Figure 6: As on Fig. 5, but an expanded view for 1996. In the right panel the y-component of the "predicted" transport $C\mathbf{W}$ is overplotted (thin line) over the "measured" T_y (thick), while the wind components U (blue) and V (red) are shown in the inset.

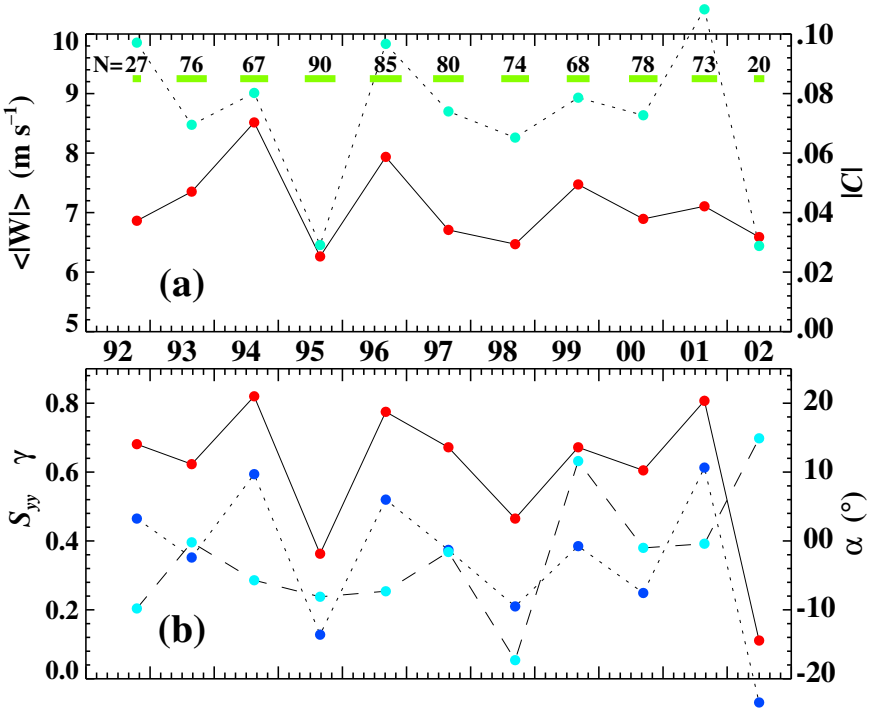

Figure 7: (a) Mean wind speed (solid line), transfer coefficient $|C|$ (dotted); (b) correlation coefficient S_{yy} (solid), hindcast skill γ (dotted), and rotation angle α (dashed), for ice-free seasons in 1992–2002. Duration of each data period and number of TP sections (N) are shown in (a).